

Dynamical Kondo effect and Kondo destruction in effective models for quantum-critical heavy fermion metals

Ang Cai,¹ Haoyu Hu,¹ Kevin Ingersent,² Silke Paschen,^{3,1} and Qimiao Si¹

¹*Department of Physics and Astronomy, Rice Center for Quantum Materials, Rice University, Houston, Texas, 77005, USA*

²*Department of Physics, University of Florida, Gainesville, Florida, 32611-8440, USA*

³*Institute of Solid State Physics, Vienna University of Technology, 1040 Vienna, Austria*

(Dated: December 15, 2024)

Quantum criticality in certain heavy-fermion metals is believed to go beyond the Landau framework of order-parameter fluctuations. In particular, there is considerable evidence for Kondo destruction: a disappearance of the *static* Kondo singlet amplitude that results in a sudden reconstruction of Fermi surface across the quantum critical point and an extra critical energy scale. This effect can be analyzed in terms of a dynamical interplay between the Kondo and RKKY interactions. In the Kondo-destroyed phase, a well-defined Kondo resonance is lost, but Kondo singlet correlations remain at nonzero frequencies. This dynamical effect allows for mass enhancement in the Kondo-destroyed phase. Here, we elucidate the dynamical Kondo effect in Bose-Fermi Kondo/Anderson models, which unambiguously exhibit Kondo-destruction quantum critical points. We show that a simple physical quantity—the expectation value $\langle \mathbf{S}_f \cdot \mathbf{s}_c \rangle$ for the dot product of the local (f) and conduction-electron (c) spins—varies smoothly across such quantum critical points. A nonzero $\langle \mathbf{S}_f \cdot \mathbf{s}_c \rangle$ manifests the dynamical Kondo effect that operates in the Kondo-destroyed phase. The implications of our results are discussed for the stability of Kondo-destruction quantum criticality as well as the understanding of experimental results in quantum critical heavy-fermion metals.

I. INTRODUCTION

Quantum criticality is a unifying theme for strongly correlated systems, driving properties such as non-Fermi liquid (“strange metal”) behavior and unconventional superconductivity [1–4]. It often develops in bad metals (*i.e.*, metals with strong correlations) and near antiferromagnetic order. Antiferromagnetic quantum critical points (QCPs) are especially prevalent in heavy-fermion metals [4–7], which are highly tunable due to their small energy scales. One of the overarching questions is whether quantum criticality in heavy-fermion systems goes beyond the Landau framework of order-parameter fluctuations, as proposed in terms of Kondo destruction [8–10]. At a Kondo-destruction QCP, a new type of critical modes arises from the suppression of the *static* Kondo singlet amplitude. Some of the salient properties associated with Kondo destruction have been experimentally observed, and are in sharp contrast with the expectations of the conventional spin-density wave QCP [11–13]. These properties include spin dynamics obeying an anomalous scaling [14], charge dynamics that are singular with ω/T scaling [15], as well as a Fermi surface that undergoes a sudden reconstruction across the QCP [16–20]. In the Kondo-destroyed phase, the Fermi surface is small, its volume being determined by the number of conduction (c) electrons only. In the Kondo phase, by contrast, the c electrons near the Fermi energy are hybridized with f electrons, and there is a large Fermi surface whose volume is determined by the combined number of c and f electrons.

Microscopically, Kondo destruction in Kondo lattice models originates from the dynamical competition between the Kondo and Ruderman-Kittel-Kasuya-Yosida (RKKY) exchange interactions. We consider the case

when both these interactions are antiferromagnetic. The Kondo interaction between each local f moment and its on-site conduction electrons lowers the ground-state energy through the development of Kondo singlet correlations, while the RKKY interaction does so by establishing singlet correlations between different local moments and the associated antiferromagnetic ordering. When the Kondo interaction dominates, the ground state features Kondo entanglement and absence of long-range antiferromagnetic order, but antiferromagnetic correlations nonetheless remain. Likewise, when the RKKY interaction prevails, the ground state displays antiferromagnetic order and destruction of ground-state Kondo entanglement, but, dynamically, Kondo correlations remain. A Kondo-destruction QCP has been realized in Kondo lattice models when the dynamical competition between the Kondo and RKKY interactions is taken into account [8, 21–25]. The dynamical Kondo effect helps stabilize a Kondo-destroyed phase and allows for the quantum phase transition from the Kondo phase to be second order [26, 27].

A. Specific motivation

The dynamical Kondo effect implies that the quasiparticles near the small Fermi surface in the Kondo-destroyed phase have enhanced mass. This is important for understanding properties such as the enhancement of the Sommerfeld coefficient (C_{el}/T), cyclotron mass, and quadratic-in- T coefficient A of the electrical resistivity ($\rho = \rho_0 + AT^2$) in the Kondo-destroyed phase implicated in YbRh₂Si₂, Au-doped CeCu₆, CeRhIn₅ and Ce₃Pd₂₀Si₆ [18–20, 28, 29].

This effect is in contrast to the expectations from a

static mean-field picture for the Kondo lattice, which reduces the Kondo correlations to just a static amplitude, say the condensation amplitude of a slave boson [30], and ignores its quantum fluctuating part. Viewed from this static mean-field perspective, destruction of the Kondo effect would imply the complete decoupling of the local-moment and conduction-electron spins, with a vanishing expectation value $\langle \mathbf{S}_f \cdot \mathbf{s}_c \rangle$ and the absence of mass enhancement for quasiparticles near the small Fermi surface.

To be more specific, by the dynamical Kondo effect, we refer to antiferromagnetic correlations at nonzero frequencies between the local-moment and conduction-electron spins in the Kondo-destroyed phase. Such correlations can be quantified in terms of the cross susceptibility

$$\chi_{Ss}(\tau) = \langle T_\tau \mathbf{S}_f(\tau) \cdot \mathbf{s}_c(0) \rangle. \quad (1)$$

The spectral function $\text{Im} \chi_{Ss}(\omega)$ is the imaginary part of the retarded correlation function $\chi_{Ss}(\omega) = \chi_{Ss}(i\omega_n \rightarrow \omega + i0^+)$, with $\chi_{Ss}(i\omega_n) = \int_0^\beta e^{-i\omega_n \tau} \chi_{Ss}(\tau) d\tau$. The dynamical Kondo effect means that $\text{Im} \chi_{Ss}(\omega)$ is nonzero for $\omega \neq 0$ in the Kondo-destroyed phase.

Consider now $\langle \mathbf{S}_f \cdot \mathbf{s}_c \rangle$, which is the equal-time limit of $\chi_{Ss}(\tau)$: $\langle \mathbf{S}_f \cdot \mathbf{s}_c \rangle = \chi_{Ss}(\tau \rightarrow 0^+)$. It relates to the spectral function $\text{Im} \chi_{Ss}(\omega)$ as follows:

$$\langle \mathbf{S}_f \cdot \mathbf{s}_c \rangle = \frac{1}{\pi} \int_{-\infty}^{\infty} n_B(\omega) \text{Im} \chi_{Ss}(\omega) d\omega, \quad (2)$$

where $n_B(\omega) = 1/(e^{\beta\omega} - 1)$ is the Bose-Einstein distribution function.

It follows from Eq. (2) that the dynamical Kondo effect implies a nonzero $\langle \mathbf{S}_f \cdot \mathbf{s}_c \rangle$ in the Kondo-destroyed phase. This motivates us to use $\langle \mathbf{S}_f \cdot \mathbf{s}_c \rangle$ as a diagnostic for the dynamical Kondo effect. We therefore calculate this expectation value in well-defined models, for which the existence of Kondo destruction can be unambiguously established. An added impetus for the present work is the recent development of an SU(2) continuous-time quantum Monte Carlo (CT-QMC) method [31] (see also Ref. 32), which is able to reach low-enough temperatures and study Kondo destruction in models with SU(2) symmetry.

B. Main results

In this paper, we study several models: the Bose-Fermi Kondo (BFK) and Bose-Fermi Anderson (BFA) Hamiltonians in their SU(2) spin-symmetric and Ising spin-anisotropic variants. We provide unambiguous evidence for the existence of a continuous quantum phase transition between Kondo-entangled and Kondo-destroyed phases that possess, respectively, nonzero and zero amplitudes for the static Kondo singlet. Our results for $\langle \mathbf{S}_f \cdot \mathbf{s}_c \rangle$ and (in the Ising-anisotropic case) $\langle S_f^z s_c^z \rangle$ show

that these quantities are nonzero even in the Kondo-destroyed phase, where the static Kondo effect is absent. Through Eq. (2), we can conclude that the dynamical Kondo effect operates in the Kondo-destroyed phase.

C. Outline of the paper

Section II describes the BFA models with either SU(2) symmetry or Ising anisotropy, and the corresponding BFK models that arise in the limit of infinite f -site Coulomb repulsion. These models emerge from the treatment of the Kondo/Anderson lattice models [8, 21–25] within the extended dynamical mean-field theory (EDMFT) [33–35] and, thus, they represent effective models for quantum-critical heavy fermion metals. In the EDMFT, one focuses on a single lattice site and integrates out all other sites, obtaining an effective model with a local f level coupled both to a fermionic bath (capturing the Kondo interaction) and a bosonic bath (representing the dynamical effect of the RKKY interaction). The competition between Kondo and RKKY interactions in the lattice model is translated into a competition between couplings to the fermionic and bosonic baths of the effective models.

There are several ways to systematically examine the quantum phase transitions of the BFA and BFK models. Analytically, the models can be studied under an ϵ -expansion renormalization-group (RG) approach. Here, the system is either in a Kondo-screened or Kondo-destroyed phase, depending on whether the system flows to a fixed point with strong Kondo coupling (which signifies the development of nonzero amplitude for the static Kondo singlet in the system's ground state [30]) or to a fixed point with vanishing Kondo coupling (which is the unambiguous evidence for the suppression of the static Kondo singlet amplitude in the ground state). Numerically, the models can be studied using CT-QMC and, in cases with Ising anisotropy, also with the NRG method. These two numerical methods usually complement each other since CT-QMC is exact but is limited to temperatures $T > 0$, while the NRG can work directly at $T = 0$ but (for nonzero temperatures) is unreliable in the frequency regime $0 < |\omega| \leq T$.

Section III focuses on the existence of Kondo destruction in the BFA and BFK models. The evidence comes from a combination of (i) analytical ϵ -expansion RG analysis of the BFK models, revealing unstable Kondo-destruction fixed points separating Kondo-screened and Kondo-destroyed phases; (ii) numerical evidence for the crossing and scaling collapse of the Binder ratio in the Ising-anisotropic BFA model; (iii) divergence of the fidelity susceptibility in both the Ising-anisotropic and SU(2) symmetric BFA; (iv) the bifurcation of the flow of the many-body spectrum in NRG calculations towards those of the Kondo-screened and Kondo-destroyed fixed points, for the Ising-anisotropic case; and (v) the collapse of quasiparticle weight as the Kondo-destruction QCP is

approached from either phase, as evidenced by the collapse of a crossover energy scale.

The central results of our work are presented in Sec. IV, which demonstrates the dynamical Kondo effect. We show that $\langle \mathbf{S}_f \cdot \mathbf{s}_c \rangle$ is nonzero in the Kondo-destroyed phase, and clarify that this captures the dynamical Kondo effect. In particular, we demonstrate that this expectation value evolves smoothly from the Kondo screened phase across the QCP into the Kondo-destroyed phase. Finally, we discuss our results in Sec. V and provide a summary of the paper in Sec. VI.

II. MODELS AND METHODS

This section describes the models considered in this work. The Bose-Fermi Kondo model with either SU(2) symmetry or Ising anisotropy has been studied analytically using the ϵ -expansion RG [33, 36–39]. The ϵ -expansion results serve as a guide for our numerical analyses, which are performed for the BFA model. The BFA model with SU(2) symmetry or Ising anisotropy reduces to the corresponding BFK model in the limit of infinite on-site repulsion between localized (f) electrons.

A. Bose-Fermi Kondo models

The SU(2)-symmetric BFK Hamiltonian can be written

$$\begin{aligned} \mathcal{H}_{\text{BFK}}^{\text{SU}(2)} &= J \mathbf{S}_f \cdot \mathbf{s}_c + g \sum_p \mathbf{S}_f \cdot (\vec{\phi}_p + \vec{\phi}_{-p}^\dagger) \\ &+ \sum_{p,\sigma} \epsilon_p c_{p\sigma}^\dagger c_{p\sigma} + \sum_p w_p \vec{\phi}_p^\dagger \cdot \vec{\phi}_p, \end{aligned} \quad (3)$$

where a spin- $\frac{1}{2}$ local moment \mathbf{S}_f is coupled both to a fermionic bath $c_{p\sigma}$ through Kondo coupling J and to a vector bosonic bath $\vec{\phi}_p$ with coupling g .

The Ising-anisotropic BFK model is specified by the Hamiltonian

$$\begin{aligned} \mathcal{H}_{\text{BFK}}^{\text{Ising}} &= J_z S_f^z s_c^z + \frac{1}{2} J_\perp (S_f^+ s_c^- + H.c.) + \sum_{p,\sigma} \epsilon_p c_{p\sigma}^\dagger c_{p\sigma} \\ &+ g \sum_p S_f^z (\phi_p^z + \phi_{-p}^{z\dagger}) + \sum_p w_p \phi_p^z \phi_p^z, \end{aligned} \quad (4)$$

where the local moment couples to the fermionic bath through longitudinal and perpendicular Kondo couplings J_z and J_\perp , and couples via the z of its spin to a single component bosonic bath. We assume isotropic bare Kondo couplings $J_z = J_\perp = J$, but within the ϵ -expansion approach one must allow for the possible development of anisotropy under RG flow.

B. Bose-Fermi Anderson models

For the purposes of CT-QMC study, it is preferable to study the BFA counterparts of the models just described. The SU(2)-symmetric BFA Hamiltonian is

$$\begin{aligned} \mathcal{H}_{\text{BFA}}^{\text{SU}(2)} &= \sum_\sigma \epsilon_d d_\sigma^\dagger d_\sigma + U n_\uparrow n_\downarrow + \sum_{p,\sigma} (V d_\sigma^\dagger c_{p,\sigma} + H.c.) \\ &+ \sum_{p,\sigma} \epsilon_p c_{p\sigma}^\dagger c_{p\sigma} + g \sum_p \mathbf{S}_f \cdot (\vec{\phi}_p + \vec{\phi}_{-p}^\dagger) \\ &+ \sum_p w_p \vec{\phi}_p^\dagger \cdot \vec{\phi}_p. \end{aligned} \quad (5)$$

with $\mathbf{S}_f = d_\sigma^\dagger \boldsymbol{\tau}_{\sigma\sigma'} d_{\sigma'}$, $n_\sigma = d_\sigma^\dagger d_\sigma$, and $\boldsymbol{\tau}_{\sigma\sigma'}$ being the vector of Pauli matrices.

The Ising-anisotropic variant of the BFA model has Hamiltonian

$$\begin{aligned} \mathcal{H}_{\text{BFA}}^{\text{Ising}} &= \sum_\sigma \epsilon_d d_\sigma^\dagger d_\sigma + U n_\uparrow n_\downarrow + \sum_{p,\sigma} (V d_\sigma^\dagger c_{p,\sigma} + H.c.) \\ &+ \sum_{p,\sigma} \epsilon_p c_{p\sigma}^\dagger c_{p\sigma} + g \sum_p S_f^z (\phi_p^z + \phi_{-p}^{z\dagger}) \\ &+ \sum_p w_p \phi_p^z \phi_p^z \end{aligned} \quad (6)$$

where $S_f^z = \frac{1}{2}(n_\uparrow - n_\downarrow)$ and n_σ as defined above.

The SU(2)-symmetric and Ising-anisotropic BFA models reduce to their BFK counterparts in the limit $U \rightarrow \infty$, $\epsilon_d \rightarrow -\infty$ of suppressed charge fluctuations on the f site. Unless the limit is taken in such a way that $U = -2\epsilon_d$, the BFK Hamiltonians are supplemented by a potential scattering term of the form $W \sum_{p,p',\sigma} c_{p,\sigma}^\dagger c_{p',\sigma}$. However, the coupling W proves to be marginal under RG flow, and it can safely be neglected.

C. Choice of fermionic and bosonic baths

To complete the models specified in Eqs. (3)–(6), it is necessary to specify the densities of states of the fermionic and bosonic baths.

For the fermionic bath, we set the density of states

$$\rho_F(\epsilon) = \sum_p \delta(\epsilon - \epsilon_p) = N_0 \Theta(|D - \epsilon|) \quad (7)$$

to be constant over a bandwidth $2D$, which leads to a hybridization function $\Gamma(\epsilon) = \Gamma_0 \Theta(|D - \epsilon|)$, with $\Gamma_0 = \pi N_0 V^2$.

The density of states for the bosonic bath is chosen to be sub-ohmic with a power-law exponent $0 < s < 1$, written as

$$\rho_B(\omega) = \sum_p \delta(\omega - \omega_p) = K_0^2 (\omega/\omega_c)^s \Theta(\omega) f(\omega/\omega_c), \quad (8)$$

with $f(x)$ being an upper cutoff function. In CT-QMC, we choose a soft upper cutoff $f(x) = \exp(-x)$,

and K_0 is determined from the normalization condition $\int_0^\infty \rho_B(\omega) = 1$. In the NRG, we choose a hard upper cutoff $f(x) = \Theta(1 - x)$.

III. KONDO-DESTRUCTION QUANTUM CRITICALITY

In this section we demonstrate the existence of a Kondo-destruction quantum phase transition in the BFK and BFA models with SU(2) symmetry and Ising anisotropy.

A. SU(2) symmetry

We first consider Kondo destruction in Bose-Fermi models that exhibit full SU(2) spin rotation symmetry.

1. ϵ -expansion RG for the BFK model

To set the stage for our analysis, we briefly recall the RG analysis via expansion in $\epsilon = 1 - s$ [36–39]. To order ϵ^2 , the RG beta functions are [36]

$$\begin{aligned}\beta(J) &= -J \left[(N_0 J) - \frac{(N_0 J)^2}{2} \right] - J [-(K_0 g)^2 + (K_0 g)^4], \\ \beta(g) &= -g \left[\frac{\epsilon}{2} - (K_0 g)^2 + (K_0 g)^4 - \frac{(N_0 J)^2}{2} \right].\end{aligned}\quad (9)$$

These RG equations yield two stable fixed points: the Kondo fixed point (K) at $g = 0$ and large J , and the local-moment fixed point (L) at $J = 0$ and intermediate g . The equations also predict one unstable fixed point (C), which is the critical point at which Kondo destruction occurs. Figure 1(a) illustrates the RG flows for the case $\epsilon = 0.1$.

2. CT-QMC treatment of the BFA model

The SU(2)-symmetric BFA model can be solved using a recently developed extension of the CT-QMC method [31, 32]. We fix the fermionic bath half-bandwidth $D = 1$, bosonic bath cutoff $\omega_c = 1$, and remain at the particle-hole symmetric point $U = -2\epsilon_d = 0.1$. The prefactor K_0 is determined from the normalization condition $\int_0^\infty \rho_B(\omega) d\omega = 1$. We choose the bosonic bath exponent to be $s = 0.6$, hold constant the bosonic coupling at $g = 0.5$, and use the amplitude of the hybridization function Γ_0 as our tuning parameter.

We can calculate the fidelity susceptibility χ_F^λ and use its divergence to detect a quantum phase transition. We consider the Hamiltonian as comprising two parts, $H = H_0 + \lambda H_1$, with λ being a tuning parameter (here H_1 is independent of λ). At zero temperature we define

the fidelity as the ground state wave-function overlap at parameters λ and $\lambda + d\lambda$,

$$F(\lambda, d\lambda) = \langle \Psi_0(\lambda + d\lambda) | \Psi_0(\lambda) \rangle. \quad (10)$$

The fidelity susceptibility can be expressed as

$$F(\lambda, d\lambda \rightarrow 0) = 1 - \frac{1}{2} \chi_F^\lambda(\lambda) d\lambda^2. \quad (11)$$

At nonzero temperature, χ_F^λ is defined as [40]

$$\chi_F^\lambda(T) = \int_0^{\beta/2} (\langle T_\tau H_1(\tau) H_1 \rangle - \langle H_1 \rangle^2) \tau d\tau, \quad (12)$$

where β is the inverse temperature $\beta = 1/T$.

At a QCP, $\chi_F^\lambda(T)$ will diverge as $\chi_F^\lambda(T) \sim \beta^{2/\nu}$. Therefore χ_F^λ can be used to detect the location of the QCP.

Here we choose the tuning parameter λ to be the hybridization V , and calculate χ_F^V vs Γ_0 at various temperatures using the method for CT-QMC introduced in Ref. 41, as shown in Fig. 1(b). We see that as a function of Γ_0 , the fidelity susceptibility develops a peak near $\Gamma_0 = 0.1$. To confirm its divergence behavior, we can perform finite-size scaling according to

$$\chi_F^V(\Gamma_0, \beta) = \beta^{2/\nu} \tilde{\chi} \left(\beta^{1/\nu} (\Gamma_0 - \Gamma_c) / \Gamma_c + A / \beta^{\phi/\nu} \right). \quad (13)$$

The collapsed data are plotted in Fig. 3(c). We find $\Gamma_c = 0.08(1)$ and $\nu^{-1} = 0.24(4)$, consistent with the ϵ -expansion result $\nu^{-1} = \epsilon/2 + \epsilon^2/6 + O(\epsilon^3) \simeq 0.23$.

B. Ising anisotropy

We now turn to Kondo destruction in Bose-Fermi models with Ising spin rotational symmetry.

1. ϵ -expansion RG for the BFK model

We again recall the RG analysis of the Ising-anisotropic BFK model, which in this case can be carried out by ϵ -expansion in a kink-gas representation [33, 36]. The RG equations are given in terms of stiffness constants κ_j , κ_g and a fugacity y_j , which are related to the bare Hamiltonian parameters by

$$\begin{aligned}\kappa_j &= \left[1 - \frac{1}{\pi} \tan^{-1} \left(\frac{\pi}{4} N_0 J_z \right) \right]^2 \\ \kappa_g &= \frac{\Gamma(\gamma)}{4} \tau_0^{1-\gamma} (K_0 g_z)^2 \\ y_j &= \frac{N_0 J_\perp}{2}.\end{aligned}\quad (14)$$

The corresponding RG beta functions are given by [33]

$$\begin{aligned}\beta(\kappa_j) &= 4\kappa_j y_j^2 \\ \beta(\kappa_g) &= -\kappa_g (\epsilon - 4y_j^2) \\ \beta(y_j) &= -y_j (1 - \kappa_j - \kappa_g/2).\end{aligned}\quad (15)$$

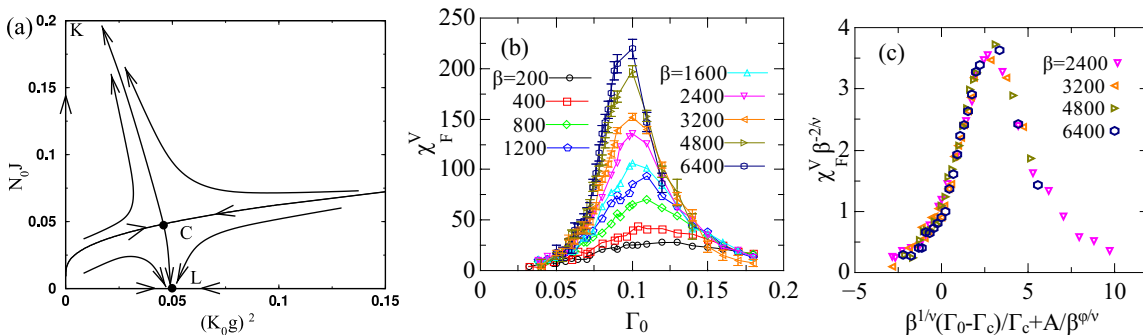


FIG. 1: (a) RG flows on the g - J plane for the SU(2) BFK model with $\epsilon = 0.1$, adapted from Ref. 36. (b) Fidelity susceptibility vs Γ_0 for the SU(2) BFA model at fixed bosonic coupling $g = 0.5$. (c) Finite-size scaling of the data in (b), plotted according to Eq. (13).

The RG flow on the y_j - κ_g plane is shown in Fig. 2(a). We find two stable fixed points: the Kondo fixed point (K) at $\kappa_g = 0$ and large y_j , and the local-moment fixed point (L) at $y_j = 0$ and large k_g . There is also one unstable fixed point (C), which is the Kondo-destruction critical point.

2. CT-QMC calculation of BFAM

We use the same parameters as in the SU(2) symmetric case to perform the CT-QMC calculations. Similar calculations have been performed previously for the case with a pseudogap [42].

The quantity that evidences a second-order phase transition in CT-QMC is the Binder ratio [43]

$$U_2 = \frac{\langle m_z^4 \rangle}{\langle m_z^2 \rangle^2}, \quad (16)$$

where $m_z = \frac{1}{\beta} \int_0^\beta S_z(\tau) d\tau$.

U_2 has the properties that $U_2 = 3$ deep in the Kondo-screened phase where the distribution of m_z is Gaussian centered around 0, and $U_2 = 1$ deep in the local moment phase where the distribution of m_z is two delta functions centered around $\pm 1/2$. Also, it is defined in such a way that, at a QCP, it should have scaling dimension exactly equal to 0, thereby becoming independent of temperature. Thus, a QCP is a point where U_2 vs Γ_0 curves at different β have a crossing.

The numerical result for Binder ratio vs Γ_0 is shown in Fig. 2(b), where we can clearly observe a crossing around $\Gamma_0 = 0.07$; see Fig. 2(c) for a zoomed-in view. According to the argument given above, this crossing suggests the existence of a quantum phase transition between a local-moment phase at small Γ_0 (where $U_2 \rightarrow 1$) and a Kondo-screened phase at large Γ_0 (where $U_2 \rightarrow 3$). We can further perform finite-size scaling according to

$$U_2(\Gamma_0, \beta) = \tilde{U}_2 \left(\beta^{1/\nu} (\Gamma_0 - \Gamma_c) / \Gamma_c + A / \beta^{\phi/\nu} \right). \quad (17)$$

Here, ν is the correlation length exponent, Γ_c is the critical value of Γ_0 , while A and ϕ represent subleading corrections to the scaling. The collapsed data are plotted in Fig. 2(d). We extract a critical hybridization width $\Gamma_c = 0.07(1)$ and a correlation-length exponent $\nu^{-1} = 0.51(4)$. The latter value is consistent with a previous NRG study of the corresponding BFK model [42], where $\nu^{-1} = 0.509(1)$ was reported.

We also confirm the existence of a Kondo-destruction QCP by calculating the fidelity susceptibility χ_F^V vs Γ_0 at various temperatures, as shown in Fig. 3(a). The fidelity susceptibility, as a function of Γ_0 , is peaked near $\Gamma_0 = 0.07$. The collapsed data under finite-size scaling are plotted in Fig. 3(b). We find $\Gamma_c = 0.07(1)$ and $\nu^{-1} = 0.50(4)$, consistent with the result from the Binder ratio.

3. NRG study of the BFA model

In this subsection, we present results for the Ising BFA model obtained using the NRG, which complements the CT-QMC by working directly at $T = 0$. The existence of distinct phases and quantum phase transitions can be seen from the flow of the many-body spectrum as a function of the NRG iteration number N . We work with a fermionic half-bandwidth $D = 1$ and a bosonic bath cutoff $\omega_c = 1$, use the same bosonic bath exponent $s = 0.6$ as in the CT-QMC calculations, and work with fixed Hamiltonian couplings $U = -2\epsilon_d = 0.2$ and $K_0g = 1.026$. The NRG discretization parameter Λ is chosen to be $\Lambda = 9$, the bosonic occupation of each Wilson chain site is capped at 8, and up to 500 many-body charge (“isospin”) multiplets are retained after each NRG iteration. With these parameter choices, we find that the QCP is located at $\Gamma_0 = \Gamma_c = 0.1$.

We plot the scaled NRG spectrum $E(N)$ vs iteration number N in Fig. 4. Here, $E(N)$ is the many-body energy at iteration N divided by $D\Lambda^{-N/2}$, the characteristic energy scale of site N on the Wilson fermionic chain, such that $E(N+2) = E(N)$ at an RG fixed point. Figure

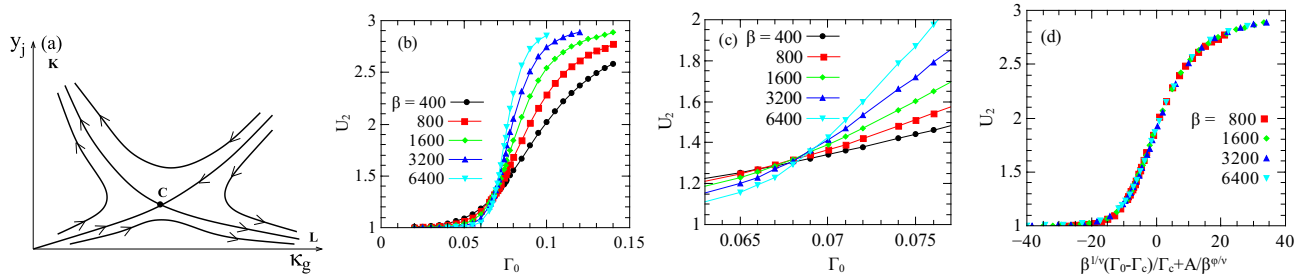


FIG. 2: (a) Schematic RG flow diagram for the Ising BFK model, adapted from Ref. 36. (b) Binder ratio U_2 vs Γ_0 for the Ising BFAM at fixed bosonic coupling $g = 0.5$. (c) Zoom-in of U_2 vs Γ_0 near the crossing point. (d) Finite-size scaling of the Binder ratio in (c), plotted according to Eq. (17). These results provide evidence for the existence of a QCP and a Kondo-destroyed phase, consistent with the analytical prediction in (a) from the ϵ -expansion RG.

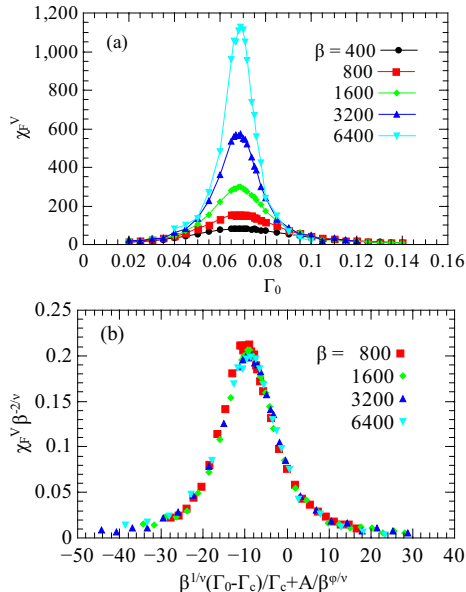


FIG. 3: (a) Fidelity susceptibility vs Γ_0 for the Ising BFAM at fixed bosonic coupling $g = 0.5$. (b) Finite size-scaling of the data in (a), demonstrating the divergence of the fidelity susceptibility and the associated scaling collapse, both providing evidence for the existence of a QCP. These results provide a consistency check for the QCP and the Kondo-destruction phase implicated by the crossing and scaling of the Binder ratio in Fig. 2.

4(a) shows the NRG flow of the lowest excited state at different distances $\Delta\Gamma_0 = \Gamma_0 - \Gamma_c$ from the QCP, specifically, $\Delta\Gamma_0 = \pm 10^{-p}$ with $p = -2, -3, \dots, -6$. The bifurcation of the energy flows in the figure clearly manifests the existence of a QCP. Close to the QCP, the scaled energy of these states approaches $E(N) = 0.167$ for the first 10 iterations or so. In the Kondo phase ($\Gamma_0 > \Gamma_c$), $E(N)$ then rises up to somewhere around 0.366, corresponding to the value for a free boson, whereas in the local-moment phase ($\Gamma_0 < \Gamma_c$), $E(N)$ descends toward zero.

Figure 4(b) plots several low-lying excited states for hybridization widths Γ_0 slightly below ($\Delta\Gamma_0 = -10^{-5}$)

and above ($\Delta\Gamma_0 = 10^{-5}$) the critical value $\Gamma_c = 0.1$. The many-body eigenstates are labeled by their values of S_z (z component of the total spin) and J (total isospin, an $SU(2)$ quantum number whose z component represents the total fermionic occupancy measured from half-filling). At intermediate iterations $N \simeq 15$, we are accessing the quantum-critical spectrum for both cases before the flow goes to the Kondo fixed-point structure or the local-moment fixed-point structure at large iteration numbers $N > 20$.

In the NRG, we can determine a crossover scale $T^* = D\Lambda^{-N^*}/2$ on both the Kondo-screened and Kondo-destroyed sides from the flow of the bosonic energy levels shown in Fig. 4(a). We plot T^* vs Γ_0 on linear scales in Fig. 4(c), demonstrating that T^* is vanishing as approaching the QCP from both sides. This provides direct evidence for Kondo destruction. Figure 4(d) is a log-log plot of T^* vs $|\Gamma_0 - \Gamma_c|$ that shows that T^* vanishes in a power-law fashion. Since this energy scale characterizes the crossover from the quantum-critical regime to the Fermi-liquid regime of the local moments, it is a measure of the quasiparticle weight Z . In other words, as the QCP is approached from the Kondo-destroyed side (as well as when it is approached from the Kondo-screened side), Z goes continuously to zero.

IV. DYNAMICAL KONDO EFFECT

We now turn to the calculation of $\langle \mathbf{S}_f \cdot \mathbf{s}_c \rangle$ and $\langle S_f^z s_c^z \rangle$. We show that these expectations values are nonzero in the Kondo-destroyed phase, and draw implications of this result for the dynamical Kondo effect.

A. Nonzero $\langle \mathbf{S}_f \cdot \mathbf{s}_c \rangle$ and $\langle S_f^z s_c^z \rangle$ in Kondo-destroyed phase

We present the CT-QMC results for $\langle \mathbf{S}_f \cdot \mathbf{s}_c \rangle$ in the $SU(2)$ BFA model and $\langle S_f^z s_c^z \rangle$ in the Ising-anisotropic BFA model in Figs. 5(a) and 5(b), respectively. The calculation is performed using the same set of parameters

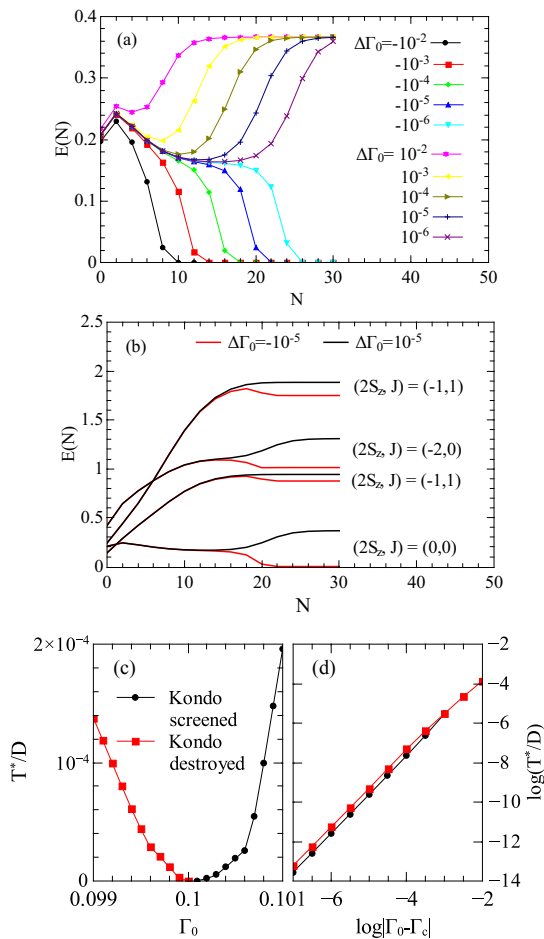


FIG. 4: NRG data for the Ising BFA model with $s = 0.6$. (a) Flow of the lowest NRG excited-state energy vs iteration number N for different values $\Gamma_0 - \Gamma_c = \pm 10^{-p}$ with $p = -2, -3, \dots, -6$. (b) Several excited states $E(N)$ vs even iteration number N for Γ_0 slightly below and above the critical coupling $\Gamma_c = 0.1$, labeled by their quantum numbers S_z (z component of total spin) and J (total isospin). (c) Crossover temperature T^* vs Γ_0 over a broad range on a linear plot, demonstrating the vanishing of T^* at the QCP at $\Gamma_0 = 0.1$. (d) Power-law behavior of the crossover scale T^* in the vicinity of the QCP, showing data in the Kondo-screened phase (red squares) and the Kondo-destroyed phase (black circles).

as in the previous section, where a Kondo-destruction QCP was identified in each model. We see that $\langle \mathbf{S}_f \cdot \mathbf{s}_c \rangle$ and $\langle S_f^z s_c^z \rangle$ are continuous at the corresponding QCPs ($\Gamma_0 = 0.08$ in the SU(2) case and $\Gamma_0 = 0.07$ in the Ising case, respectively) and stay finite in the local moment phase and only approaches 0 when the hybridization parameter Γ_0 goes to zero. We do not observe much variation across different temperatures.

For the Ising-anisotropic BFA model, using NRG we can calculate both $\langle S_f^z s_c^z \rangle$ and $\langle \mathbf{S}_f \cdot \mathbf{s}_c \rangle$ at $T = 0$. The evolution of the two quantities as functions of tuning parameter Γ_0 , for both the Kondo-destroyed phase ($\Gamma_0 <$

$\Gamma_c = 0.1$) and Kondo-screened phase ($\Gamma_0 > \Gamma_c = 0.1$), is shown in Fig. 5(c). We find that $\langle S_f^z s_c^z \rangle$ and $\langle \mathbf{S}_f \cdot \mathbf{s}_c \rangle$ are continuous across the QCP ($\Gamma_0 = \Gamma_c$). These observations are consistent with the results derived by CT-QMC at nonzero temperatures. By performing the calculation at different choice of U and ϵ_d , we also find that the values of $\langle S_f^z s_c^z \rangle$ and $\langle \mathbf{S}_f \cdot \mathbf{s}_c \rangle$ at the transition are not universal numbers of the QCP but depend on the underlying microscopic parameters of the model, which determine where the phase boundary is crossed.

Figure 5 represents the central result of our work, namely the expectation values $\langle \mathbf{S}_f \cdot \mathbf{s}_c \rangle$ and $\langle S_f^z s_c^z \rangle$ are nonzero in the Kondo-destroyed phase. As stressed earlier, based on Eq. 2 and its analogue for $\langle S_f^z s_c^z \rangle$, these nonzero expectation values imply that the spectral functions $\text{Im} \chi_{S_s}(\omega)$ and $\text{Im} \chi_{S_s^z}^z(\omega)$ are nonzero at nonzero frequencies, signifying the dynamical Kondo effect in the Kondo-destroyed phase.

B. Signature of the transition

While these expectation values are smooth across the QCP, we show that their derivative with respect to the control parameter manifests the transition. For this purpose, we define the non-linear susceptibility X_K^z for $\langle S_f^z s_c^z \rangle$ as well as X_K for $\langle \mathbf{S}_f \cdot \mathbf{s}_c \rangle$ as follows

$$X_K = -\frac{\partial \langle \mathbf{S}_f \cdot \mathbf{s}_c \rangle}{\partial \Gamma_0}, \quad (18)$$

$$X_K^z = -\frac{\partial \langle S_f^z s_c^z \rangle}{\partial \Gamma_0}. \quad (19)$$

In Figs. 6(a) and 6(b), we plot X_K for the SU(2) BFA model and X_K^z for the Ising-anisotropic BFA model across the corresponding QCP determined from the calculations using CT-QMC. We see that while $\langle \mathbf{S}_f \cdot \mathbf{s}_c \rangle$ and $\langle S_f^z s_c^z \rangle$ are smooth across the QCP, their derivatives X_K and X_K^z show peaks that manifest the underlying QCPs.

The corresponding result from the NRG at $T = 0$ is shown in Fig. 6(c). We see that X_K^z and X_K are increasing as we approach the QCP from both sides. This suggests that they will be peaked at the QCP, in agreement with the trend towards lower temperatures shown in the CT-QMC result.

V. DISCUSSION

Several remarks are in order. First, we have shown that $\langle \mathbf{S}_f \cdot \mathbf{s}_c \rangle$ is nonzero in the Kondo-destroyed phase of BFK and BKA models. The robustness of this result can also be seen as follows. Consider, for definiteness, the SU(2) BFK model, Eq. (3). Here, $J \mathbf{S}_f \cdot \mathbf{s}_c$ is a term in the Hamiltonian. We can view J as an external source field, with $\mathbf{S}_f \cdot \mathbf{s}_c$ being its conjugate. This is in analogy to the case of a Zeeman coupling, where magnetization is the conjugate to an external magnetic field. Similar

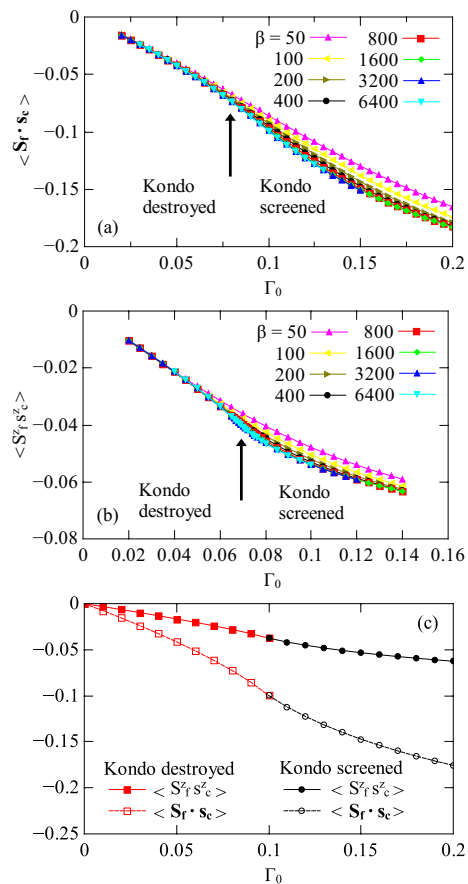


FIG. 5: (a) $\langle \mathbf{S}_f \cdot \mathbf{s}_c \rangle$ vs Γ_0 for the SU(2) BFK model at fixed bosonic bath coupling $g = 0.5$. The arrow marks the QCP at Γ_c , which separates the Kondo destroyed ($\Gamma_0 < \Gamma_c$) and Kondo screened ($\Gamma_0 > \Gamma_c$) regions. (b) $\langle S_f^z s_c^z \rangle$ vs Γ_0 in the Ising BFA model at fixed bosonic bath coupling $g = 0.5$. The legends parallel those of panel (a). (c) $\langle S_f^z s_c^z \rangle$ (solid squares and circles) and $\langle \mathbf{S}_f \cdot \mathbf{s}_c \rangle$ (open squares and circles) vs Γ_0 in the Ising BFAM at fixed bosonic bath coupling obtained by NRG at $T = 0$. The red and black regions respectively correspond to the Kondo destroyed ($\Gamma_0 < \Gamma_c$) and Kondo screened ($\Gamma_0 > \Gamma_c$) sides of the QCP.

to an external magnetic field leading to a nonzero magnetization, we expect $\langle \mathbf{S}_f \cdot \mathbf{s}_c \rangle$ to be generically nonzero in the presence of a nonzero J , including in the Kondo-destroyed phase.

Second, that $\langle \mathbf{S}_f \cdot \mathbf{s}_c \rangle$ is smooth across the transition means that this quantity is not a suitable diagnostic of the Kondo-destruction QCP. Instead, the existence of the Kondo-destruction quantum phase transition is seen through other means. These include the ϵ -expansion with RG flow to the Kondo-destroyed state, crossing and scaling collapse of the Binder ratio, the divergence and scaling collapse of the fidelity susceptibility, a bifurcation in the NRG many-body spectra, and a vanishing crossover energy scale when the QCP is approached from either side. These results provide evidence for a continuous quantum phase transition, where the amplitude of the

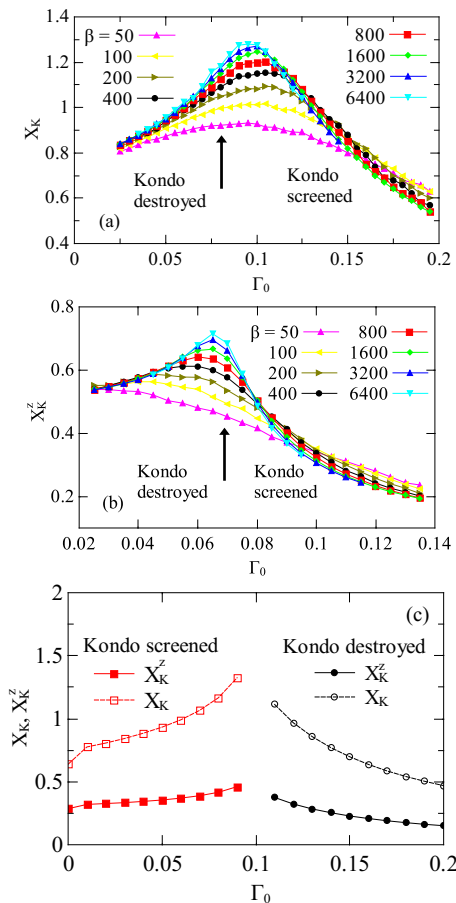


FIG. 6: (a) Nonlinear susceptibility X_K vs Γ_0 for the SU(2) BFK model at fixed bosonic bath coupling $g = 0.5$. (b) Nonlinear susceptibility X_K^z vs Γ_0 for the Ising BFA model at fixed bosonic bath coupling $g = 0.5$. (c) Nonlinear susceptibilities $X_{f_c}^z$ and X_{f_c} vs Γ_0 for the Ising BFAM at fixed bosonic bath coupling obtained by NRG at $T = 0$.

static Kondo singlet smoothly goes from nonzero in the Kondo-screened phase to zero in the Kondo-destroyed phase. For example, the ϵ -expansion RG shows that the Kondo-destroyed phase has a vanishing Kondo coupling, signifying a vanishing amplitude for the static Kondo singlet. However, along the trajectory *during the flow towards the fixed point*, the effective Kondo coupling is nonzero and gives rise to the dynamical Kondo effect.

Third, through EDMFT, the Kondo lattice model is solved in terms of an effective BFK model in the presence of a local magnetic field [8, 21–25]. Such studies have identified a continuous Kondo-destruction quantum phase transition, where a self-consistently determined local magnetic field rises continuously from zero as the system enters the Kondo-destroyed phase. The results presented here imply that $\langle \mathbf{S}_f \cdot \mathbf{s}_c \rangle$ will be smooth across the Kondo-destruction QCP in the Kondo lattice case.

Fourth, we emphasize that in the Kondo lattice problem, the dynamical Kondo effect is crucial for stabilizing the Kondo-destroyed phase, namely, the antiferromag-

netic state with a small Fermi surface, referred to as AF_S in the literature [44]. When the dynamical Kondo effect is neglected, AF_S would not be energetically favored. For instance, in variational quantum Monte Carlo studies [45], the energy gain from the Kondo coupling only shows up in the form of a static Kondo amplitude of the trial wave-function, which is zero in the AF_S phase. The expectation value $\langle \mathbf{S}_f \cdot \mathbf{s}_c \rangle$ vanishes in the AF_S phase. Thus, such a variational quantum Monte Carlo approach cannot capture the dynamical Kondo effect and the AF_S is absent in this approach.

VI. SUMMARY

We have calculated the expectation value for the product of the local moment and conduction-electron spins in $SU(2)$ -symmetric and Ising anisotropic Bose-Fermi Anderson models where Kondo-destruction quantum-critical points are unambiguously identified. Our key results are given in Fig. 5, which shows this expectation value to vary smoothly across the Kondo-destruction quantum critical points. Through a spectral decomposition, this nonzero expectation value demonstrates the dynamical Kondo effect that operates in the Kondo-destroyed phase. This dynamical Kondo effect is important for the stability of Kondo-destruction quantum criticality. In addition, it provides understanding of the

enhanced effective mass in the Kondo-destroyed phase implicated in quantum-critical heavy fermion materials such as $YbRh_2Si_2$, Au-doped $CeCu_6$, $CeRhIn_5$, and $Ce_3Pd_{20}Si_6$.

VII. ACKNOWLEDGMENTS

We thank E. M. Nica for useful discussions. This work was supported in part by the NSF under Grant Nos. DMR-1611392 (A.C., Q.S.) and DMR-1508122 (K.I.), and by the Robert A. Welch Foundation C-1411 (H.Y.). Computing time was supported in part by the Data Analysis and Visualization Cyberinfrastructure funded by NSF under grant OCI-0959097 and an IBM Shared University Research (SUR) Award at Rice University, and by the Extreme Science and Engineering Discovery Environment (XSEDE) by NSF under Grant No. DMR-170109. S.P. acknowledges funding from the Austrian Science Fund (project P29296-N27) and from the European Union's Horizon 2020 research and innovation programme under grant agreement No. 824109. Q.S. acknowledges hospitality and support under a Ulam Scholarship from the Center for Nonlinear Studies at Los Alamos National Laboratory, and the hospitality of the Aspen Center for Physics, which is supported by NSF grant No. PHY-1607611.

-
- [1] Special Issue on Quantum Criticality and Novel Phases, *Physica Status Solidi (b)* **250**, 417 (2013).
 - [2] Special issue on Quantum Phase Transitions, *J. Low Temp. Phys.* **161**, 1 (2010).
 - [3] S. Sachdev, *Quantum phase transitions* (Cambridge university press, 2011).
 - [4] Q. Si and F. Steglich, *Science* **329**, 1161 (2010).
 - [5] P. Coleman and A. J. Schofield, *Nature* **433**, 226 (2005).
 - [6] G. Stewart, *Reviews of modern Physics* **73**, 797 (2001).
 - [7] Q. Si and S. Paschen, *physica status solidi (b)* **250**, 425 (2013).
 - [8] Q. Si, S. Rabello, K. Ingersent, and J. L. Smith, *Nature* **413**, 804 (2001).
 - [9] P. Coleman, C. Pépin, Q. Si, and R. Ramazashvili, *J. Phys. Cond. Matt.* **13**, R723 (2001).
 - [10] T. Senthil, M. Vojta, and S. Sachdev, *Phys. Rev. B* **69**, 035111 (2004).
 - [11] J. A. Hertz, *Physical Review B* **14**, 1165 (1976).
 - [12] A. Millis, *Physical Review B* **48**, 7183 (1993).
 - [13] T. Moriya, *Spin fluctuations in itinerant electron magnetism*, vol. 56 (Springer Science & Business Media, 2012).
 - [14] A. Schröder, G. Aeppli, R. Coldea, M. Adams, O. Stockert, H. Löhneysen, E. Bucher, R. Ramazashvili, and P. Coleman, *Nature* **407**, 351 (2000).
 - [15] L. Prochaska, X. Li, D. MacFarland, A. Andrews, M. Bonta, E. Bianco, S. Yazdi, W. Schrenk, H. Detz, A. Limbeck, et al., arXiv preprint arXiv:1808.02296 (2018).
 - [16] S. Paschen, T. Lühmann, S. Wirth, P. Gegenwart, O. Trovarelli, C. Geibel, F. Steglich, P. Coleman, and Q. Si, *Nature* **432**, 881 (2004).
 - [17] S. Friedemann, N. Oeschler, S. Wirth, C. Krellner, C. Geibel, F. Steglich, S. Paschen, S. Kirchner, and Q. Si, *Proc. Natl. Acad. Sci. USA* **107**, 14547 (2010).
 - [18] H. Shishido, R. Settai, H. Harima, and Y. Ōnuki, *Journal of the Physical Society of Japan* **74**, 1103 (2005).
 - [19] J. Custers, K. Lorenzer, M. Müller, A. Prokofiev, A. Sidorenko, H. Winkler, A. Strydom, Y. Shimura, T. Sakakibara, R. Yu, et al., *Nature Materials* **11**, 189 (2012).
 - [20] V. Martelli, A. Cai, E. Nica, M. Taupin, A. Prokofiev, C.-C. Liu, H.-H. Lai, R. Yu, R. Küchler, A. Strydom, D. Geiger, et al., arXiv preprint arXiv:1709.09376 (2017).
 - [21] Q. Si, S. Rabello, K. Ingersent, and J. L. Smith, *Physical Review B* **68**, 115103 (2003).
 - [22] D. Grempel and Q. Si, *Physical review letters* **91**, 026401 (2003).
 - [23] J.-X. Zhu, D. Grempel, and Q. Si, *Physical review letters* **91**, 156404 (2003).
 - [24] M. T. Glossop and K. Ingersent, *Physical review letters* **99**, 227203 (2007).
 - [25] J.-X. Zhu, S. Kirchner, R. Bulla, and Q. Si, *Physical review letters* **99**, 227204 (2007).
 - [26] Q. Si, J. H. Pixley, E. Nica, S. J. Yamamoto, P. Goswami, R. Yu, and S. Kirchner, *Journal of the Physical Society of Japan* **83**, 061005 (2014).
 - [27] J.-X. Zhu, D. Grempel, and Q. Si, *Physical review letters*

- 91**, 156404 (2003).
- [28] P. Gegenwart, J. Custers, C. Geibel, K. Neumaier, T. Tayama, K. Tenya, O. Trovarelli, and F. Steglich, *Phys. Rev. Lett.* **89**, 056402 (2002).
- [29] H. v. Löhneysen, T. Pietrus, G. Portisch, H. G. Schlager, A. Schröder, M. Sieck, and T. Trappmann, *Phys. Rev. Lett.* **72**, 3262 (1994).
- [30] A. C. Hewson, *The Kondo Problem to Heavy Fermions* (Cambridge University Press, Cambridge, 1997).
- [31] A. Cai and Q. Si, arXiv preprint arXiv:1902.10094 (2019).
- [32] J. Otsuki, *Physical Review B* **87**, 125102 (2013).
- [33] Q. Si and J. L. Smith, *Physical review letters* **77**, 3391 (1996).
- [34] J. L. Smith and Q. Si, *Physical Review B* **61**, 5184 (2000).
- [35] R. Chitra and G. Kotliar, *Physical review letters* **84**, 3678 (2000).
- [36] L. Zhu and Q. Si, *Physical Review B* **66**, 024426 (2002).
- [37] G. Zaránd and E. Demler, *Physical Review B* **66**, 024427 (2002).
- [38] J. Smith and Q. Si, *EPL (Europhysics Letters)* **45**, 228 (1999).
- [39] A. M. Sengupta, *Physical Review B* **61**, 4041 (2000).
- [40] A. F. Albuquerque, F. Alet, C. Sire, and S. Capponi, *Physical Review B* **81**, 064418 (2010).
- [41] L. Wang, Y.-H. Liu, J. Imriška, P. N. Ma, and M. Troyer, *Physical Review X* **5**, 031007 (2015).
- [42] J. Pixley, S. Kirchner, K. Ingersent, and Q. Si, *Physical Review B* **88**, 245111 (2013).
- [43] K. Binder, *Zeitschrift für Physik B Condensed Matter* **43**, 119 (1981).
- [44] Q. Si, *Physica B: Condensed Matter* **378**, 23 (2006).
- [45] H. Watanabe and M. Ogata, *Physical review letters* **99**, 136401 (2007).